Initiation of Stress Corrosion Cracking in Cold-Drawn Prestressing Steel in Hardened Cement Mortar Exposed to Chlorides

Dyana Joseline, Radhakrishna G. Pillai,‡,* and Lakshman Neelakantan***

Cold-drawn, high-strength, prestressing (PS) steel strands are widely used in pretensioned concrete (PTC) structures. This paper discusses the stress corrosion cracking (SCC) of PS steel embedded in cement mortar and gradually exposed to chlorides. Various stages of the passive to active (P-to-A) transition, which marks the onset of SCC, were investigated using the electrochemical impedance spectroscopy technique. The key mechanisms were identified and confirmed using scanning electron microscopy/energy dispersive x-ray analysis, x-ray diffarction, and confocal Raman spectroscopy. It was found that the passive film on unstressed PS steel has better electrochemical characteristics than that on conventional steel rebars. However, the residual tensile stress at the surface of PS steels can assist passive film cracking after chloride attack—contrary to the pitting corrosion without cracking of passive film in conventional steels. Further, tests indicated that the concentration of chlorides required to crack the passive film in PS steels can reduce by about 50% when prestressed—as in field structures. Chemical composition, stress state, and microstructural features at the PS steel surface were identified as possible factors influencing the initiation of SCC in PTC structures.

KEY WORDS: corrosion, chloride, durability, prestressed concrete, service life, steel, strand, stress corrosion cracking

INTRODUCTION

Chloride-induced corrosion is one of the main causes of premature deterioration of reinforced concrete and pretensioned concrete (PTC) structures. Although the exposure to chloride ions and their ingress through the cover concrete could be similar, the progress of corrosion is reported to be more insidious in PTC systems,[1] with localized corrosion and wire breakage being recurrent observations from failed PTC structures.[2-4] The mechanism of strand deterioration is still being debated. As early as 1971, it was reported that hydrogen embrittlement/hydrogen embrittlement stress cracking was the proven cause of 35% of brittle failures in prestressed concrete structures.[5-6] Later, in 2001, an exhaustive review of literature on corrosion of PS steels was presented by the American Concrete Institute (ACI) committee 222.2R,[7] with a conclusion that relatively few failures of PTC structures can be attributed to stress corrosion cracking (SCC) and hydrogen embrittlement compared to pitting. However, in 2003, the International Federation for Structural concrete (*fib*) stated that pure brittle failures because of the notch effect of corrosion pits are rare in PTC systems and that the failure is predominantly attributed to hydrogen-induced SCC, where the hydrogen is supplied by the cathodic reaction of the corrosion process. "Insufficiently present alkaline protection and/or depassivation after chloride attack" were reported to be the major causes of deterioration and even steel failure.[8]

Based on failure analysis of a corroded PTC viaduct with cold-drawn prestressed steel of strength grade 1,800 MPa, Vehovar, et al.,[9] reported that the cause of failure was SCC in the presence of chloride ions and supported by hydrogen. Chloride ions can locally damage the passive film and lead to corrosion of the depassivated regions, where the metal (M) dissolves anodically to form M^{n+}, which together with chlorides form corrosion products. The metal ions can then hydrolyze, reducing the local pH (Equation [1]) and preserving the conditions under which active dissolution of the steel strand can take place.

$$M^{+}Cl^{-} + H_2O \rightarrow MOH + H^{+}Cl^{-} \quad (1)$$

In prestressed bridge structures exposed to deicing salts and marine environments, the local pH within naturally formed pits can be 1.5 to 6.0, i.e., much lower than 12.5 to 13.2 in the bulk cementitious matrix.[6] The cathodic reaction (hydrogen evolution reaction) generates a coverage of hydrogen on the surface of the steel (adsorbed hydrogen [H_{ad}]), which may either get adsorbed into the material as diffusible hydrogen or get released as H_2 gas. Further, cold drawing-induced shear cracks in the pearlitic PS steel are reported to be potential hydrogen trapping sites.[10-12] Based on the brittle service failures exhibited by pearlitic steels in general, Novokshchenov[6] postulated (in the introduction) that "sensitivity to cracking appears to be an inherent characteristic of high-strength steels and is believed to be associated with the manufacturing processes that increase strength." In addition to the aforementioned mechanism, cathodic protection of PTC structures may also lead to hydrogen embrittlement,[13-15] although not evaluated in this study. The

Submitted for publication: November 1, 2020. Revised and accepted: May 24, 2021. Preprint available online: May 28, 2021, https://doi.org/10.5006/3730.
‡ Corresponding author. E-mail: pillai@civil.iitm.ac.in.
* Department of Civil Engineering, Indian Institute of Technology Madras, Chennai India, 600 036.
** Corrosion Engineering and Materials Electrochemistry Laboratory, Department of Metallurgical and Materials Engineering, Indian Institute of Technology Madras, Chennai India, 600 036.

ISSN 0010-9312 (print), 1938-159X (online)

research gaps, and review of literature leading to the selection of the characterization procedures used in this study (i.e., on PS steel wire in hardened cementitious systems/mortar), are presented in the following sections.

1.1 | Need for Understanding of the Initiation Phase of Stress Corrosion Cracking

Brittle failure of PS steel wires can be attributed to SCC and not just typical chloride-induced pitting/localized corrosion. The three stages during SCC are (1) crack initiation, (2) crack propagation, and (3) failure. The exact effect of hydrogen on the crack initiation in PS steels is still unclear, although some theories are available.[6,11] Nevertheless, Stage 1 is initiated by electrochemical reactions (depassivation) as discussed previously. Chlorides, in particular, have been reported to depassivate PS steels in alkaline-simulated environments and activate corrosion reactions.[16] The transition from localized corrosion to cracking can depend on the electrochemical state at the base of localized corrosion site and its geometry, chemistry of the metal, and the stress at the base of the pit. However, a conclusive relationship between these parameters is lacking due to the difficulty in the detection of the corrosion-induced crack initiation on the steel surface.[17] Sanchez, et al.,[18] summarized the three mechanisms they considered most relevant for cracking of prestressing steel in sodium bicarbonate solution: anodic dissolution, film-induced cleavage model, and surface mobility mechanism (SMM). These mechanisms focus on the crack propagation (Stage 2). Also, among these only the SMM "incorporates the effect of hydrogen produced during the process" and provides an "extension of the theory on SCC to hydrogen embrittlement."[18] However, it is to be noted that this environment is a substantial deviation from chloride induced corrosion in concrete (more relevant for carbonated concrete); the pH is much lower (buffered around 8) and the depassivating chloride is not present. Stages 2 and 3 may be influenced by the stress intensity at the crack tip and the local electrochemistry.

Majority of the available literature on SCC in PS steels are on mechanisms governing Phases 2 and 3 of SCC with the evaluation of performance based on testing of precracked or notched steel samples in various aggressive solutions.[7,18-29] Although investigations on Phases 2 and 3 based on standard tests, as per recommendations of the International Federation of Prestressed Concrete (FIP) and the Deutsches Institut für Bautechnik (DIBt), may suffice to check the suitability of any new type of high-strength steel for usage as reinforcement in PTC,[28,30] Sanchez, et al.,[18] and others[29,31] have suggested that the introduction of the first phase by generating a pit electrochemically would be more ideal. It can thus be said that the use of standardized tests is not a problem if the corrosion process is taking place at a SCC crack tip, unless hydrogen in the bulk is needed, in which case more heavily corroded wire will behave differently (as suggested by Vu, et al.[16]).

In-service failure of PTC structures due to SCC generally occurs after several years post corrosion initiation, i.e., after passive-to-active (P-to-A) transition. Therefore, P-to-A transition is a decisive stage of the initiation of the SCC process. Vélez, et al.,[32] have reported a distinct difference between the open-circuit potential (E_{corr}) and polarization resistance (R_p, determined using linear polarization resistance technique) measured at passive and active stages of chloride-induced corrosion of strands in concrete. They conclude, by using literature on conventional rebars as benchmark, that early corrosion of strands occurs at a higher rate than the former and attribute it to crevice corrosion because of the geometry of the strand. However, this corrosion rate can also be attributed to the pitting corrosion in the topmost wires, whose contribution cannot be separated from the overall electrochemical response, in a prestressed strand-concrete system. Therefore, this study utilizes a single PS steel wire to capture the passive film breakdown, as well as the pit initiation. Karuppanasamy and Pillai[33] reported estimates on the corrosion rate of quenched and self-tampered (QST) and PS wire during the corrosion propagation phase. However, their focus was on estimation of time required for corrosion-induced cracking of concrete cover and hence, they do not highlight tracking of P-to-A transition in their study. An investigation on how the chloride-induced P-to-A transition takes place in PS steel embedded in cementitious systems, and whether it is similar to that reported in conventional rebars, can aid in better understanding of the initiation of SCC in PTC systems due to chlorides, which begins with depassivation and subsequent metal dissolution.

1.2 | Preconditioning, Passivation, Chloride Exposure, and Characterization

Typically, metallographic samples are subjected to surface grinding prior to corrosion testing to eliminate variations in the metal substrate.[34-39] However, such surface preparation can also result in removal of surface features, thereby making the sample not representative of the field scenario.[40] This is particularly critical in PS steel because the first step towards manufacturing is acid cleaning of the parent rod followed by rinsing and immersion in hot aqueous solution of zinc phosphate, borate, or lime. This coating has the potential to protect the surface and enhance bonding of the cold drawing lubricants.[7] Díaz, et al., reported that zinc phosphate, the most common chemical used in the production line of PS steel, offers primary protection against atmospheric corrosion and can break down under the influence of applied tensile stress.[41] Hence, for realistic understanding of the P-to-A transition, the PS steel samples should ideally be used in the as-received condition,[41-42] which is followed in this study.

Further, steel embedded in concrete forms a passive film in the highly alkaline environment provided by the hardened concrete. While the passive film gets fully developed over many years in the PTC structures, it is not the case in laboratory specimens. Potentiostatically formed (say, artificially in laboratory) passive films on carbon steel, in alkaline environments, are reported to be much different than those formed under open-circuit conditions (naturally in the PTC structures), with the former films being less protective than the latter.[35] Also, several studies on the corrosion behavior of PS steels have used simulated pore solutions (SPS) of various formulations (say, (i) $Ca(OH)_2$,[42] (ii) cement extract,[41] (iii) $Ca(OH)_2$+NaOH+KOH,[36] and (iv) KOH+NaOH+$CaSO_4{\cdot}2H_20$+$Ca(OH)_2$[43]) to mimic the cementitious environment. The electrochemical parameters and chloride contents producing similar behavior are reported to be not comparable between steels in SPS and steels in mortar,[44] with different passivation kinetics due to variation in pH and ion mobility, physical nature of the interface, etc.[45] Further, different pore solutions (say, $Ca(OH)_2$ vs. $Ca(OH)_2$ + NaOH + KOH + $Ca(SO_4)$) can result in passive films with different atomic structures.[46] Depassivation of steel in cementitious environment is also dependent on factors specific to both the steel and binder type—such as quality and pH of steel/concrete interface,[47] which cannot be accounted for using SPS. Also, most studies in SPS do not consider the transient nature of chloride

exposure, with the chloride concentration being precalculated as against progressive and slow build-up in the actual scenario.[44] Providing a cementitious passivating environment to the PS steel would be the most realistic scenario with the chloride concentration at the steel/cement interface progressively increased. In field, chloride transport in concrete is complicated and can occur by a variety of mechanisms such as diffusion due to a concentration gradient, diffusion under pressure capillary suction due to humidity gradient, etc.[48] Methods to accelerate chloride-induced corrosion in laboratory investigations are mainly impressed current, admixed chlorides, and cyclic wetting and drying, and a detailed review of the applicability of each is presented by Otieno, et al.[49] For studies on understanding corrosion mechanisms such as this one, impressed current may not be ideal. This is because the usage of external current can promote uniform corrosion (instead of localized) due to treatment of entire steel surface as anode, although the occurrence of this phenomenon could be dependent on the magnitude of the applied current. Further, the acidification of the steel/cementitious interface, in response to the applied voltage, is reported to promote corrosion even in the absence of chlorides.[50] In case of strands, initiation of crevice corrosion is also likely. Usage of admixed chlorides is also not suitable as it does not allow passivation to happen. However, during cyclic wetting and drying, the acceleration is primarily by increased chloride transport due to diffusion combined with capillary suction and replenishing dissolved oxygen at steel surface to sustain cathodic reaction. This method being as close to natural as possible, has been used in a majority of laboratory studies[51-53] and has been adapted in the present study.

Due to the presence of nontransparent mortar around the steel, the P-to-A transition cannot be visually assessed. Also, the hydrated cement mortar has a sol-gel structure[54] with partially liquid-filled pores making them a resistive electrolyte,[55] contrary to aqueous electrolytes such as SPS. This is important for using techniques to evaluate the electrochemistry at the steel/concrete interface (as discussed in Rengaraju, et al.,[55] for looking at rebar in concrete/mortar). The electrochemical impedance spectroscopy (EIS) technique is reported to be satisfactory in deciphering the individual responses of the steel, the interface, and mortar from the combined response of the steel-mortar systems over a wide range of resistivities.[39,55-57] Being nondestructive in nature, it also allows the continuous monitoring of the embedded steel in both its passive and active state through repetitive tests.[56] Furthermore, the EIS technique has gained a lot of popularity owing to its potential to characterize various processes such as passivation,[36] depassivation,[37,58] pitting,[41,59-62] and pit-to-crack transitions.[63] Hence, EIS is a promising in situ electrochemical tool to investigate the P-to-A transition in PTC systems.

The objective of this study was to understand the P-to-A transition in PTC systems exposed to chlorides due to its important role in the initiation of SCC. Therefore, a methodology which is as close to reality as possible, albeit in a laboratory scale, was framed for the investigation of the P-to-A transition. The work was performed in two phases. The first phase focused on assessing the P-to-A transition in both conventional rebars (QST) and PS steels, and characterizing the salient features. At each stage of characterization, the causative mechanisms were probed into to identify metallurgical factors playing significant roles in the P-to-A transition. Based on the observations from Phase 1 of the study, it was concluded that for a given steel, the residual stress state and the passive film quality play key roles in the P-to-A transition. Hence, the second phase of the study focused on understanding the effect of applied prestress on the P-to-A transition. Also, the chloride concentration responsible for P-to-A transition, which is defined as chloride threshold (Cl_{th}) of prestressed steel in cementitious environment is presented, which would provide a quantitative understanding on the chloride-induced P-to-A transition in actual PTC structures.

EXPERIMENTAL PROCEDURES

2.1 | Materials

Steels and cement used were procured from local producers. PS steel was supplied as 7-wire strands in coils. The central (king) wires of 5.28 mm diameter, extracted from the PS strands of nominal diameter 15.2 mm and conforming to IS 14268,[64] were used for the investigation. The ultimate tensile strength (f_{pu}) of the king wire was found to be about 1,800 MPa, which is comparable with that of the cold drawn steels used in other investigations.[1,22,44,65] A QST steel with a tempered martensite surface and ferrite-pearlite core, conforming to IS 1786[66] with a characteristic yield strength of 415 MPa and 8 mm diameter, was chosen for comparison. The elemental composition of the PS and QST steels, as determined using Metavision 108 NN+[†] emission spectrometer, is reported in Table 1. These steels were embedded in mortar made with ordinary Portland cement (OPC) conforming to IS 12269:2013.[67] The oxide composition of the OPC cement used is presented in Table 2. The cement mortar used had a water: binder:fine aggregate ratio of 0.5:1:2.75. The fine aggregate component consisted of a 50-50 mix of standard sands of Grades II and III (of particle sizes 1 mm to 0.5 mm and 0.5 mm to 0.09 mm, respectively) conforming to IS 650.[68]

Table 1. *Chemical Composition of PS and QST Steels*

Element	Concentration (wt%)	
	PS	QST
C	0.898	0.250
Si	0.194	0.378
Mn	0.716	0.660
P	<0.005	0.020
S	0.014	0.017
Cr	0.562	0.058
Ni	0.093	0.032
Cu	0.025	0.016
Al	0.032	<0.008
B	0.005	0.001
Nb	0.052	0.050
Pb	0.095	<0.020
Ti	0.055	0.005
W	0.105	<0.005
N	0.011	0.007
Remaining[(A)]	96.648	98.492

[(A)] Remaining includes Fe and other trace elements.

[†] Trade name.

Table 2. *Chemical Composition of Ordinary Portland Cement (OPC) Used in this Study*

Material	CaO	SiO_2	Al_2O_3	Fe_2O_3	MgO	Na_2O	K_2O	TiO_2	SO_3	LOI[(A)]
OPC	64.59	19.01	4.17	3.89	0.88	0.16	0.59	0.23	1.70	1.40

[(A)] LOI: Loss on ignition.

2.2 | Phase 1: P-to-A Transition in Quenched and Self-Tempered and Prestressing Steels

2.2.1 | Specimen Preparation

QST and PS steels of 100 mm length were cut using an abrasive cutter (with continuous supply of coolant). Then, the steel pieces were drilled and tapped on one end face, to fasten a stainless steel (SS) rod of 3 mm diameter. Following this, the prepared steel samples were ultrasonically cleaned (frequency: 35 kHz; power: 160 W) in distilled water for 15 min and wiped with a cotton cloth soaked with ethanol. The SS rods were then threaded onto the steel pieces, the junction was covered with heat-shrink neoprene tubing, and the steel samples were placed in a plastic tube mold. After casting with mortar and demolding, the lollipop-shaped specimens (with a mortar cover of thickness ≈10 mm to 11 mm) were capped at the bottom using epoxy and cured for 28 d in a curing chamber. Five specimens each with QST and PS steels embedded in OPC-based cement mortar were prepared. Prior to exposure, the cured specimens were dried for 5 d, during which three coats of ambient temperature cured two-part epoxy were applied on the surface of the mortar, leaving a 5 cm long region at the middle for exposure. The area of exposure of the QST and PS steels within this 5 cm long region was 12.6 cm^2 and 8.3 cm^2, respectively, and has been used in electrochemical calculations.

2.2.2 | Test Setup and Methodology

All long-term experiments were performed at an ambient temperature of 25°C. SPS of composition presented in Table 3 and pH of 12.8 was prepared at every test cycle using distilled water and reagent-grade chemicals. Then, 3.5% NaCl was added to the prepared SPS, and the resulting chloride contaminated SPS was used both as exposure solution and the test electrolyte, as utilized in previous studies.[55] The reason for using chloride containing SPS (with Ca, Na, and K salts) instead of plain chloride solution was to avoid reduction of alkalinity of the mortar cover either due to leaching of ions or carbonation.

The test setup used for the electrochemical investigation is shown in Figure 1. Circumferentially placed nichrome mesh was used as the counter electrode (CE), the steel rebar/wire was the working electrode (WE), and the saturated calomel electrode (SCE), placed between CE and WE, was the reference electrode. The specimens were exposed to chlorides by cyclic wetting and drying (5 d dry followed by 2 d wet) in SPS+3.5% NaCl. The E_{corr} of the embedded steel was monitored at the end of every wet exposure. Upon attainment of a steady state, EIS measurements were made, and the evolution pattern was used to detect corrosion initiation, which marked the end of exposure. As cement mortar is inhomogeneous, variations in the distribution of the aggregates may induce variability in the pore network of mortar cover, among the different specimens of the same set. This can affect the chloride ingress rate. Also, the unavoidable variability in the initial surface features (say roughness, residue of cold drawing chemicals in PS steel, etc.) of the as-received degreased steels used in the study may cause variations in the concentration of chlorides at the steel surface causing P-to-A transition. Hence, note that the total exposure time will vary in each specimen depending on the occurrence of P-to-A transition. For the EIS testing, Solartron Analytical 1255B† Frequency Response Analyser coupled with Solartron Analytical 1287† Electrochemical Interface was used. An AC perturbation signal of ±10 mV amplitude (peak-to-peak) was applied over a frequency range of 10^5 to 0.01 Hz at E_{corr} and 10 points per decade were recorded.

Table 3. *Chemical Composition of Simulated Pore Solution (SPS)*

Constituents	Concentration (g/L)
Distilled water	966.08
Calcium hydroxide	0.30
Sodium hydroxide	10.40
Potassium hydroxide	23.23

2.2.3 | Surface Characterization Using Scanning Electron Microscopy/Energy Dispersive X-Ray Analysis, Confocal Raman Spectroscopy, and Residual Stress Measurement

The evolution of the impedance response during the P-to-A transition was found to be different for the QST and PS steel systems. Therefore, the surfaces of the PS and QST steels extracted from the mortar were characterized using a scanning electron microscopy (SEM) for getting clarity on the phenomenon. The sampling and testing procedures are as follows. After autopsy, 1 cm long steel pieces were sampled from the 50 mm long exposed region at locations where corrosion spots/stains were visible. Note that immediately after P-to-A transition, no macroscopic sectional loss can be observed on the steel surface; but the regions undergoing active dissolution will have localized brownish corrosion stains (due to formation of corrosion products) that can be clearly discerned. Precautions were taken to ensure minimal disturbance to the surface of the steel during the sampling. Characterization of the surface using SEM and energy dispersive x-ray analysis (EDAX) was performed within 12 h from the time of extraction from the cement mortar preceded by gentle air blowing. SEM images were obtained at an accelerating voltage of 20 kV and working distance of 9.9 mm using the secondary electron detector of INSPECT F† scanning electron microscope. The corrosion products formed on the embedded QST and PS steels were also characterized using the alpha300R† raman spectrometer with a confocal setup.

The PS and QST steels vary with respect to the manufacturing processes involved; being cold drawing in the former, as opposed to QST in the latter. To understand the implication of the manufacturing process, the surface residual stresses on 50 mm long pieces of QST and PS steels, sampled

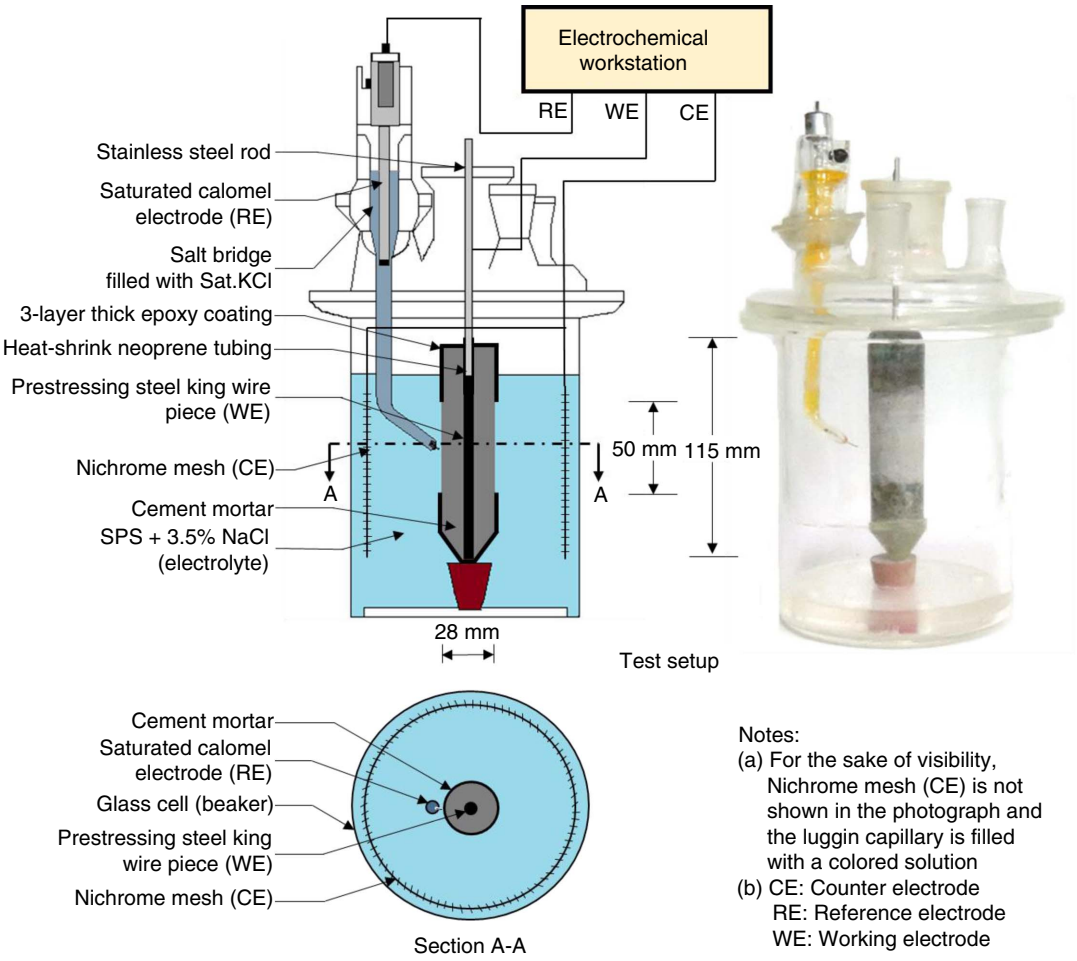

FIGURE 1. *Test Setup 1—for testing unstressed lollipop specimens.*

using electrical discharge machining, were measured with the Proto iXRD† residual stress analyser using Cr-Kα radiation.

2.3 | Phase 2: Effect of Stress on the P-to-A Transition of Prestressing Steel

2.3.1 | Specimen Preparation

To evaluate the effect of stress on the P-to-A transition, five lollipop specimens with tensioned PS steel embedded in OPC were prepared. The step-by-step procedure for specimen preparation is as follows. Self-reacting frames were fabricated for the preparation and testing of specimens with the influence of stress considered. Wedge and barrel arrangement at either end of the frame facilitated the maintenance of desired level of stress, which was applied manually based on measured strain from the steel. Cement mortar was cast over the tensioned king wire (stressed to service level prestress of 0.76 f_{pu} as per Indian Standards[69]). A specially designed cell was fixed onto the hardened mortar after 24 h, following which specimens underwent 28 d of curing with water filled into the cell. Although this is different from the curing procedure adapted for the unstressed specimens, no differences in the resulting structure of the passive film are anticipated for a cover thickness of ≈10 mm. This is because similar relative humidity condition (100% saturation) is reported to be attained within 2 d in similar OPC mortar, regardless of whether the specimens were cured in curing chamber or immersed in solution.[70] The details of the stressed test specimen with in-built cell are shown in Figure 2. A strain gauge (5 mm gauge length) was fixed on each king wire sample prior to assembling the specimen. Outward screwing of the inner hexnuts at the top side was done to impart tension to the wire until the strain corresponding to 0.76 f_{pu} (determined from stress-strain response) was measured using a data acquisition system. Wedge and barrel arrangement at either end of the frame facilitated the maintenance of stress.

2.3.2 | Testing Methodology

Because of a previous experience with very early initiation in stressed specimens resulting in less data for analysis, the concentration of NaCl used in the exposure solution was reduced to 2% for the stressed specimens. It should be noted that the specimens were under stress during the entire exposure and testing period. The chloride exposure involved cyclic wetting and drying (5 d dry-2 d wet) in SPS+2% NaCl. The exposure solution was filled into the in-built cell of the specimen during the 2 d of wetting. Only a 5 cm long region in the middle of the specimen was exposed to chlorides, similar to the unstressed specimens. EIS and E_{corr} measurements were made at the end of every wet exposure as explained in the *Test Setup and Methodology* section, and the exposure was stopped after detection of initiation. After the detection of P-to-A transition, the specimens were autopsied at the level of steel, i.e., split longitudinally into halves, and a layer of mortar

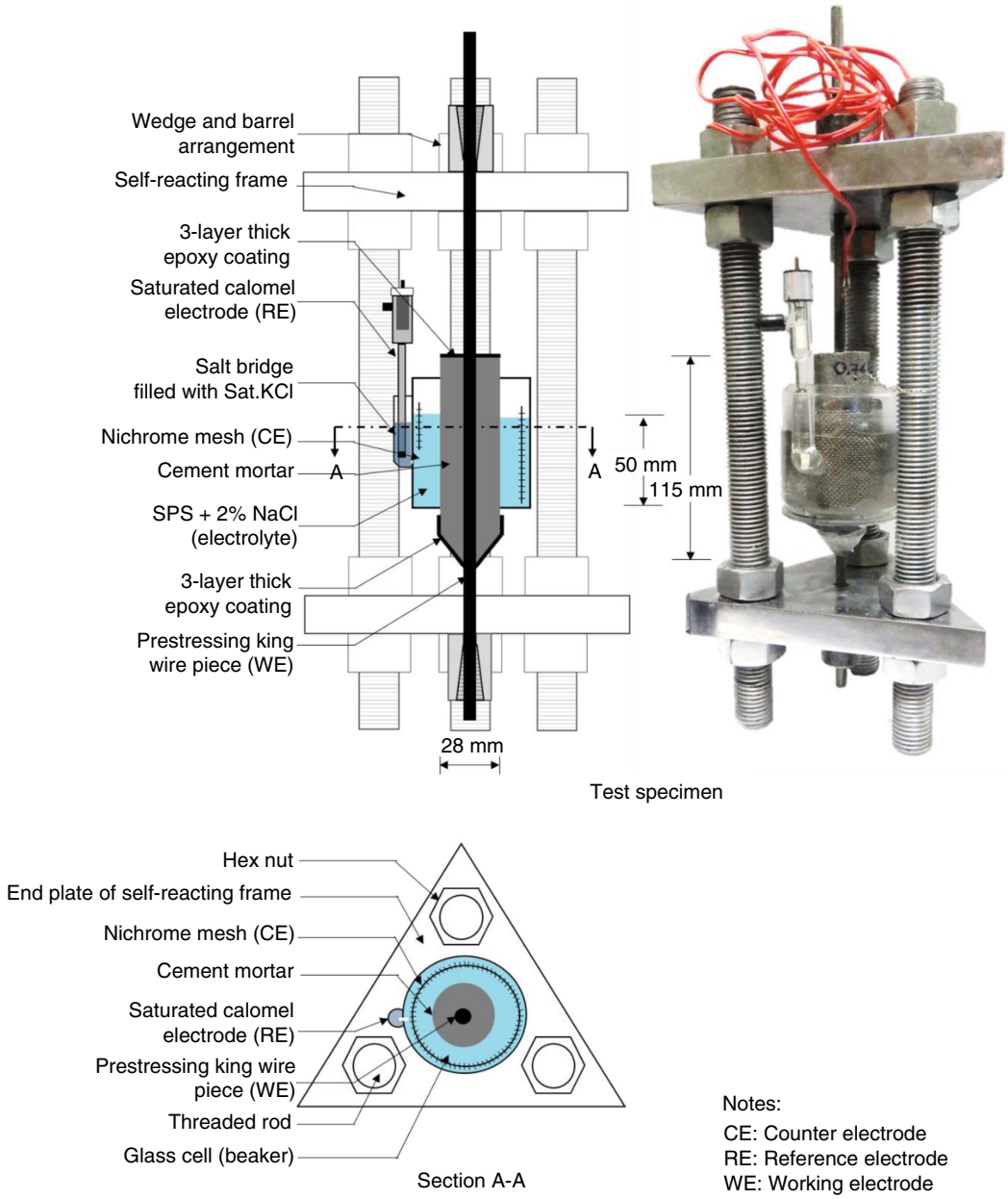

FIGURE 2. *Test Setup 2—for testing stressed lollipop specimen.*

(<1 mm deep) adjacent to the steel was extracted from the 5 cm long exposed region using a metallic round file of 5 mm diameter. The acid-soluble chloride content in the cementitious fraction of the sample was determined using chloride specific-ion probe based on the procedure outlined in SHRP S 330.[71]

RESULTS AND DISCUSSION

Periodic EIS measurements, electron micrographs, Raman spectrographs, and residual stress measurements were used to understand the P-to-A transition in QST and PS steels passivated in OPC-based cement mortar, and then subjected to chloride ingress. The effect of stress on P-to-A transition was then evaluated by electrochemical characterization (EIS and E_{corr}) followed by determination of the chloride content at the level of steel. The findings are discussed in the sections that follow.

3.1 | Phase 1: P-to-A Transition in Quenched and Self-Tampered and Prestressing Steels

3.1.1 | Electrochemical Characterization Using Electrochemical Impedance Spectroscopy

An example of the EIS response obtained from steel-mortar systems is shown in Figure 3. Unlike aqueous electrolytes, the cement mortar (a sol-gel structure[54] with partially filled pores) possesses a significant resistance that evolves with age. Depending on the frequency range of testing, three incomplete and overlapping arcs of suppressed semicircles are observed typically: each corresponding to the mortar (R_m and Q_m), double layer (R_{ct} and Q_{dl}), and the passive film (R_{ox} and Q_{ox}). Hence, a 3-RC circuit (shown in the inset of Figure 3) can be used to model the response from steel-cementitious mortar systems.[55] A higher angle of the low-frequency impedance data with respect to the real axis in the Nyquist plot can indicate

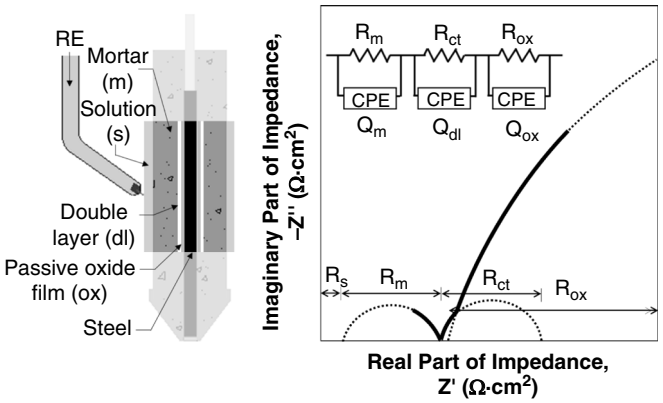

FIGURE 3. *Typical EIS response from steel-mortar systems.*

a larger arc diameter, which in turn can qualitatively indicate a higher R_{ox}. An assessment of the EIS response measured from the QST and PS steels throughout the P-to-A transition is presented herein—first qualitatively and then quantitatively.

A typical evolution of the impedance response obtained from QST steel, embedded in OPC-based mortar and subjected to cyclic wet and dry exposure to SPS+3.5% NaCl, is shown in Figures 4(a) through (c). The arc in the low-frequency region (10^{-1} to 10^{-2} Hz) in the Nyquist representation (Figure 4[a]) of the EIS response, which is indicative of the condition of the passive film, was found to have a slope greater than 45° in the initial cycles of exposure (day 7 to day 21) after 28 d of passivation during curing. The low-frequency impedance modulus ($|Z|_{0.01\ Hz}$) shown in the Bode representation (Figure 4[b]) was found to be about 10^4 Ω·cm^2.

After 35 d of exposure, a reduction in the slope of the arc in the low-frequency region was observed. This could be more evidently noted in Bode magnitude and phase responses, which show a gradual reduction in the $|Z|_{0.01\ Hz}$ and phase angle at 0.01 Hz, $\varphi_{0.01\ Hz}$, after 35 d of exposure. This hints the onset of localized depassivation of QST due to the action of chlorides. A more significant reduction in the arc diameter observed at 91 d could be due to the corrosion of steel in the depassivated regions. This is also evident in the $|Z|_{0.01\ Hz}$ and $\varphi_{0.01\ Hz}$. At this stage, $\varphi_{0.01\ Hz}$ was found to be lowered to −40°. However, it is to be noted that the reduction in the slope of the arc and $|Z|_{0.01\ Hz}$ from 35th day to 91st day is so gradual that a statistical analysis of the measured parameters is required to confirm corrosion initiation.[72-74] This could be because the corroding area (within depassivated region) is much smaller than the area in which the passive film is still intact, resulting in subtle indications of corrosion initiation in the electrochemical measurements.

On the contrary, a typical evolution of the impedance response obtained from PS steel, embedded in OPC mortar subjected to cyclic wet and dry exposure to SPS+3.5% NaCl, is shown in Figures 5(a) through (c). The pattern was found to be very different from that observed in Figure 4. Initially, the arc in the low-frequency region (10^{-1} Hz to 10^{-2} Hz) of the Nyquist representation (Figure 5[a]) indicated a large R_{ox}, with the angle of the arc with respect to real axis close to 75°. Such a response is reported by Diaz, et al.,[41] for PS steel with the angle increasing with the duration of passivation in alkaline environment. A large angle corresponds to a well-formed passive film,[36] defined as highly compact and protective. The $|Z|_{0.01\ Hz}$ shown in the Bode representation (Figure 5[b]) was found to be about 10^5 Ω·cm^2, which is one order higher than that observed in QST steel. The $\varphi_{0.01\ Hz}$ was also about −75°, which is higher than that observed in QST. The EIS spectra obtained from 7th to 49th days of exposure (after the passivation during the 28 d of curing) are characteristic of a "passive" state.

As the exposure progressed, a different type of spectrum was observed with a slightly reduced $|Z|_{0.01\ Hz}$ and an increased arc curvature observed in the Nyquist representation (56th day) indicating reduction in diameter of the semicircle (see Figure 5[a]). This could correspond to the "depassivated" state when the passive film is locally broken by the action of chlorides resulting in subtle changes in the electrochemical response as observed in QST steel. The slight reduction in the $|Z|_{0.01\ Hz}$ and $\varphi_{0.01\ Hz}$ from 49th to 56th day ascertains this observation. In the following cycles of exposure, a drastic difference in the EIS response was observed with a significant reduction in the slope of the arc (indicating very low R_{ox}) and the magnitude of $|Z|_{0.01\ Hz}$ (63rd and 70th day), indicating "active" state. The $\varphi_{0.01\ Hz}$

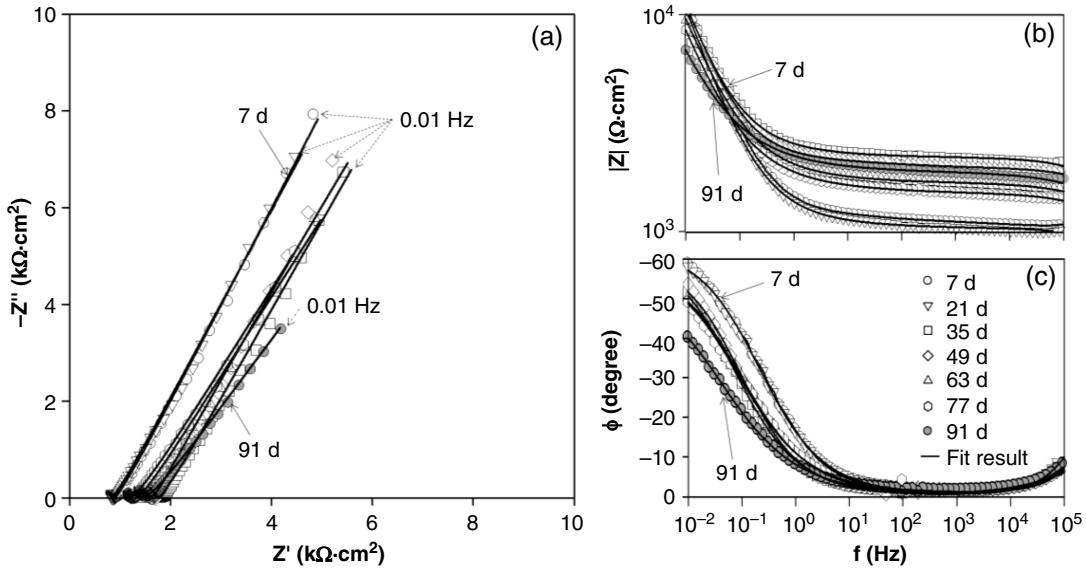

FIGURE 4. *Typical evolution of the impedance response at E_{corr} (AC amplitude: ±10 mV [peak-to-peak]) obtained at the end of wet exposure to SPS+3.5% NaCl for QST steel in OPC mortar. (a) Nyquist, (b) Bode magnitude, and (c) Bode phase representations.*

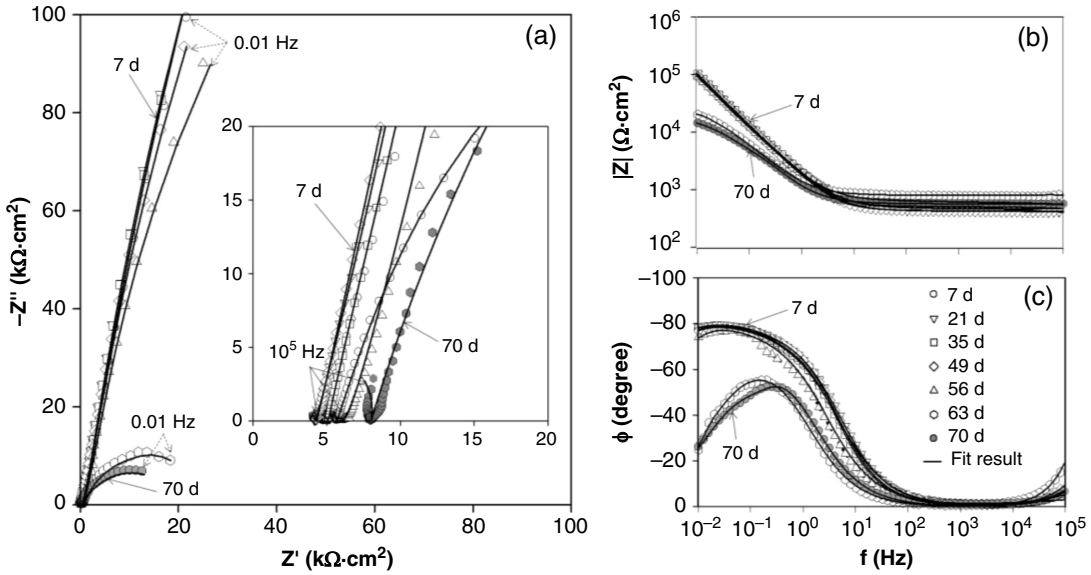

FIGURE 5. *Typical evolution of the impedance response at E_{corr} (AC amplitude: ±10 mV [peak-to-peak]) obtained at the end of wet exposure to SPS+3.5% NaCl for PS steel in OPC mortar. (a) Nyquist, (b) Bode magnitude, and (c) Bode phase representations.*

also reduced drastically from −75° to −25°, possibly indicating reduction in protectiveness of the passive layer. Typically, a phase angle of −90° indicates purely capacitive behavior and is related it to the protectiveness of oxide. Defect-free oxide is more capacitive and has barrierlike properties.

However, such a drastic change of the electrochemical response is not characteristic of chloride-induced localized pitting, as observed from the EIS and SEM results presented by Poupard, et al.,[75] for passive Fe E24 steel embedded in cementitious environment and exposed to chlorides, and can indicate a more serious deterioration of the passive film. Also, it is to be noted that $|Z|_{0.01\ Hz}$ observed after P-to-A transition in PS steel was found to be still similar in magnitude to that observed in QST in its passive state, while $\varphi_{0.01\ Hz}$ was found to be significantly low. The capacitive response of PS steel, as shown in Figure 5(c), also shifted from lower frequency (around 10^{-2} Hz) to higher frequency (about 10^{-1} Hz) after the P-to-A transition, the reason for which could be the introduction of several low-impedance pathways through the passive film during the P-to-A transition.[76] The EIS spectra obtained from the QST and PS steels throughout the P-to-A transition were fitted using a 3-RC circuit (see inset of Figure 3). The fit was found to be good as shown in Figures 4 and 5. Typical fit results and the goodness of fit, as indicated by the χ^2 value, are shown in Table 4. The variation in R_m and Q_m did not follow a particular trend; as they may be influenced by the differences in the level of saturation (does not affect low-frequency response as per Rengaraju, et al.[55]) chloride concentration in the mortar and by the pore refinement with increasing ages of mortar. Further, the frequency range studied does not allow an accurate quantification of Q_m; so, the fit results were not considered. No specific trend in the variation of R_{ct} could be identified during the P-to-A transition possibly because of the very low rates of dissolution at this stage. The reduction in Q_{dl} in the last two cycles (initiation of active stage) could be due to the slowing down of corrosion at the locations of initiation due to the presence of corrosion products. Further, it is well known that the electrode surface roughness, and variability in thickness or composition of the layer considered influence constant phase element parameters.

Comparison of the R_{ox} and Q_{ox} values obtained from QST and PS steels during P-to-A transition is presented in the sections that follow, for the sake of clarity. Also, SEM images gave insights into the difference in the evolution of EIS response from QST and PS steel systems and are discussed next.

3.1.2 | Surface Characterization Using Scanning Electron Microscopy/Energy Dispersive X-Ray Analysis, Confocal Raman Spectroscopy, and Residual Stress Measurement

A QST steel sample was extracted from the specimen whose EIS response is shown in Figure 6. The ribs in a typical QST rebar are shown in Figure 6(a) and the distributed pits observed on the steel in the vicinity of the ribs are shown in Figure 6(b). The pits were found to be covered with the corrosion product because of which they could not be clearly visualized. The sample was then ultrasonicated in ethanol, sputter coated with gold and another SEM image was collected. One of the revealed pits in the Region "B" marked in Figure 6(b), is shown in Figure 6(c), although part of it may still be covered with the corrosion products. However, the appearance of an integrated passive film with multiple pits supports the assertion that the P-to-A transition in QST steel in cementitious system happens by conventional "pitting corrosion" mechanisms. This could be the reason why the difference in the electrochemical response is subtle.

SEM image of the surface of a PS steel king wire in the "as-received condition" is shown in Figure 7(a). The rough appearance along the drawing direction can be attributed to the process of cold drawing, in which pearlitic steel rod is passed through a series of dies made of tungsten carbide—resulting in progressive reduction in diameter, and increase in yield and ultimate tensile strengths.[7,10] The surface of PS steel extracted from OPC-based mortar that was cast along-side the tested specimens, but left unexposed to chlorides is shown in Figure 7(b). The roughness of the surface is found to have visibly reduced due to the long-term passivation (98 d including the period of curing). A similar passivated surface condition is expected to have resulted in the large slope of the low-

Table 4. *Typical EIS Fit Results Showing Changes in Interfacial and Passive Film Characteristics on QST and PS Systems During the P-to-A Transition*

System/Days of Exposure		R_m (kΩ·cm^2)	R_{ct} (kΩ·cm^2)	Q_{dl} (mS·s^{n1}/cm^2)	n_1	R_{ox} (kΩ·cm^2)	Q_{ox} (mS·s^{n2}/cm^2)	n_2	χ^2
QST	7	0.08	2.01	3,700	0.27	950	660	0.71	8.0×10^{-4}
	14	0.08	1.93	3,800	0.27	950	710	0.71	1.4×10^{-3}
	21	0.08	1.93	3,800	0.28	932	710	0.71	1.4×10^{-3}
	28	0.17	1.90	3,886	0.31	363	998	0.67	5.9×10^{-3}
	35	0.14	1.89	3,030	0.29	760	740	0.70	1.2×10^{-3}
	42	0.15	0.07	3,013	0.30	431	883	0.61	1.4×10^{-3}
	49	0.11	0.18	4,150	0.42	603	670	0.69	9.8×10^{-4}
	56	0.13	1.26	2,230	0.31	712	700	0.70	9.8×10^{-4}
	63	0.10	1.25	2,840	0.28	613	777	0.67	9.7×10^{-4}
	70	0.11	1.20	1,358	0.37	602	750	0.74	1.7×10^{-3}
	77	0.11	1.19	2,200	0.20	593	900	0.67	9.5×10^{-4}
	84	0.11	1.60	960	0.49	353	850	0.78	1.6×10^{-3}
	91	0.15	1.68	1,860	0.35	153	1,250	0.66	9.2×10^{-4}
PS_0 f_{pu}	7	0.05	1.74	760	0.59	1,573	122	0.91	8.0×10^{-4}
	14	0.05	1.39	1,000	0.54	2,770	120	0.91	9.0×10^{-4}
	21	0.05	1.11	790	0.65	1,623	100	0.92	3.3×10^{-4}
	28	0.06	0.38	640	0.88	3,186	110	0.91	4.5×10^{-3}
	35	0.06	0.67	810	0.75	2,180	118	0.91	9.0×10^{-4}
	42	0.06	0.71	760	0.74	2,600	118	0.91	1.0×10^{-3}
	49	0.05	1.95	760	0.69	1,083	133	0.92	8.0×10^{-4}
	56	0.07	4.04	490	0.65	537	150	0.95	6.0×10^{-3}
	63	0.09	0.80	106	0.75	24.8	240	0.82	2.0×10^{-3}
	70	0.07	1.8	300	0.78	26.4	240	0.82	2.0×10^{-3}
PS_0.76 f_{pu}	7	0.22	1.89	0.009	0.90	3,604	62	0.90	6.9×10^{-4}
	14	0.16	1.41	0.029	0.80	3,400	62	0.90	2.6×10^{-4}
	21	0.06	1.82	0.002	0.94	446	92	0.88	3.6×10^{-4}
	28	0.22	1.84	0.007	0.94	30	119	0.96	8.8×10^{-3}
	35	0.03	0.296	7.87	0.93	5	689	0.84	3.3×10^{-2}

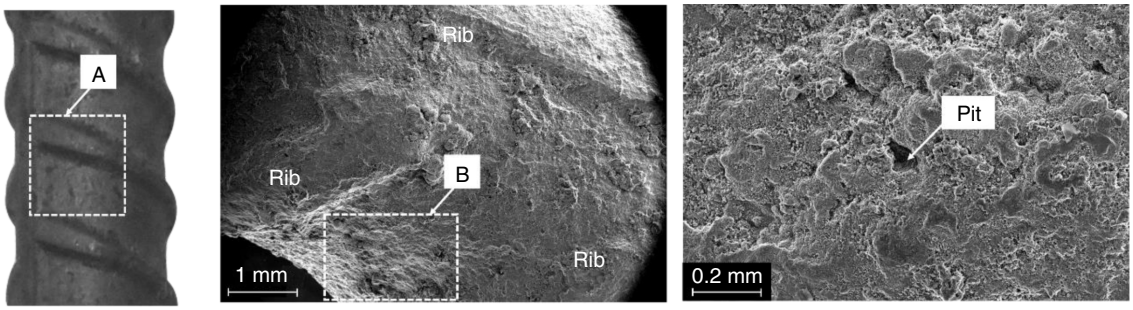

FIGURE 6. *Pitting corrosion observed on the QST rebar after 91 d of cyclic exposure to SPS+3.5% NaCl. (a) QST rebar, (b) distributed pits on QST rebar within the region "A" shown in (a), and (c) a single pit on the QST rebar within the region "B" shown in (b).*

frequency impedance response (indicating high R_{ox}) observed in the Nyquist plots shown in Figure 7 between 7 d and 49 d of exposure.

The surface of PS steel extracted from OPC-based mortar, after detection of "active" stage at the end of 70 d of cyclic exposure to SPS+3.5% NaCl, is shown in Figure 7(c).

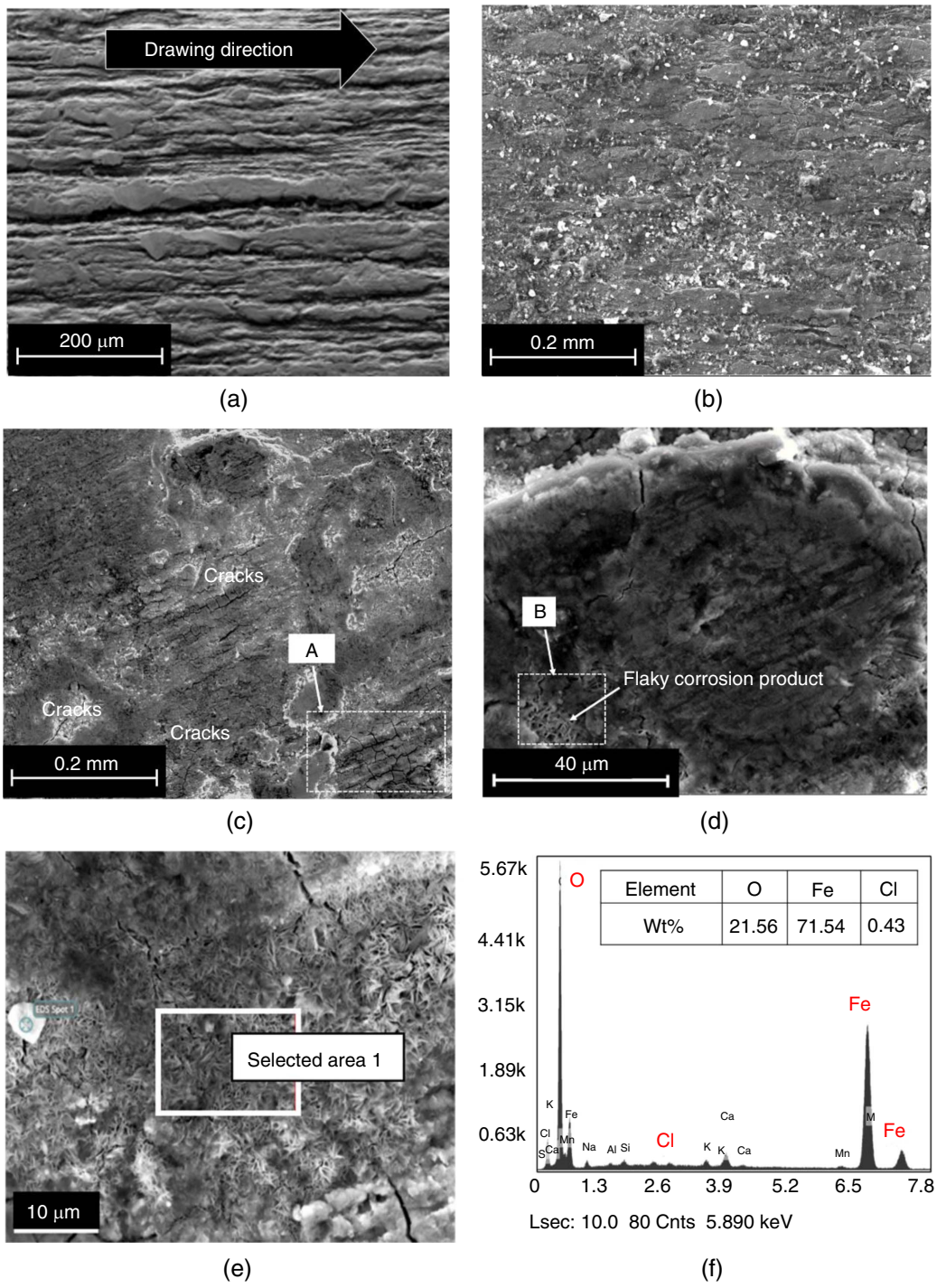

FIGURE 7. *Characterization of surface of unstressed PS steel under different conditions. (a) As-received; degreased with ethanol, (b) after 70 d of passivation in OPC-based mortar after 28 d of curing, (c) after 70 d of cyclic exposure to SPS+3.5% NaCl in OPC-based mortar after 28 d of curing, (d) enlarged view of region "A" shown in (c), (e) EDAX analysis of region "B" shown in (d), and (f) elements identified in the EDAX analysis as shown in (e).*

As expected, the drastic reduction in the arc diameter and $|Z|_{0.01\ Hz}$ was found to be due to the significant deterioration of the passive film. Microcracks following a maplike pattern were observed in multiple regions on the surface of the PS steel sample indicating the cracking of passive film. Figure 7(d) shows an enlarged view of one of the cracked regions. Corrosion product of a flaky morphology was found between the microcracks. The EDAX analysis performed on the flaky product is shown in Figures 7(e) through (f). The presence of iron, oxygen, and chloride could be detected, thereby confirming that the observed product is a result of chloride-induced corrosion. The cracking appears to have resulted from the expansive stresses exerted by the corrosion products formed at the locally "depassivated" regions on the surface of PS steel.

Other cracked regions, with similar composition, were also observed on the surface during the SEM imaging. There were also regions where the flaky product was not visible on the surface "yet" possibly due to the termination of the test immediately after the P-to-A transition.

The proposed mechanism of passive film cracking is founded on the electrochemical and micrographical evidence presented in the study. First, there was a clear distinction between the EIS spectra obtained at the passive and active stages in PS steel systems. Darowicki, et al.,[58] have reported a similar trend in the evolution of EIS response obtained from passive 304L stainless steel at E_{corr} subjected to elongation at a constant strain rate in the presence of 0.5 M NaCl, and attributed it to the cracking of passive layer due to the applied tension. Although the material and the test procedure are very different, it can be agreed upon that a large difference in the response warrants a large modification of the passivated surface, as in case of cracking of passive film. Second, micrographs (see Figure 7[c] through [f]) also indicated the presence of cracks in the passive film after P-to-A transition. While it is impossible to ascertain by imaging whether microcracks were present before the mortar was removed or not owing to the experimental complications, the authors are certain that they were not. This confidence is based on the agreement between the change in electrochemical response and the surface condition indicated in the micrographs. Also, Figure 7(b) shows a passivated PS steel surface in cement mortar of similar age but unexposed to chlorides, which does not have any cracking.

Based on the morphology, the flaky corrosion product could be edge-edge joined lepidocrocite and/or goethite crystals (refer Figure 7 of Bastidas, et al.[77]). However, because the condition of exposure of the steels in this study are different from the one referenced (extracted from cement mortar vs. long-term atmospheric exposure), Raman spectrographs were obtained to identify the phases. The Raman spectrographs of corrosion products obtained from QST and PS steels after P-to-A transition are shown in Figure 8. While peaks corresponding to hematite, lepidocrocite, goethite, and akageneite could be identified in both the samples, there could be differences in the amorphous fractions of the corrosion products. While sharp and narrow bands were predominantly observed for the corrosion product sample from PS steel, weak and broad peaks were observed for the corrosion product obtained from QST steel. This could indicate lower crystalline fractions in the corrosion product[78] obtained from QST. Crystallization pressure is generated only due to the formation of crystalline phases[79] and a high crystalline pressure (239.38 MPa to 374.99 MPa) can be generated due to the formation of various oxyhydroxides.[77] Although not a part of this study, a quantitative XRD analysis may aid in determining the contents of crystalline and amorphous phases, and verify the potential differences in the corrosion products. To further understand the reason for peculiar P-to-A transition in PS steel, the metallurgical aspects were evaluated and are elaborated in the following section.

3.1.3 | Metallurgical Aspects

The $|Z|_{0.01\ Hz}$ measured from passive QST and PS steels (at 7 d) are 11.87±1.4 kΩ·cm^2 and 105.18±11.6 kΩ·cm^2, respectively. Likewise, slope of the low-frequency Nyquist response (10^{-1} Hz to 10^{-2} Hz) with real axis, for QST and PS steels, are 59.3±3.6° and 77.2±1.29°, respectively. Based on the qualitative analysis, the passive film on PS steel clearly offers a better protection than that on QST steel initially. As expected based on the qualitative analysis of the EIS spectra, the R_{ox} of passive QST steel (950 kΩ·cm^2), shown in Table 4, was found to be lower than that of passive PS steel (1,573 kΩ·cm^2), indicating a passive film of higher resistance in the latter. On the other hand, the Q_{ox} of QST steel (mS·s^{n2}/cm^2) was higher than that of PS steel (mS·s^{n2}/cm^2), indicating difference in passive film thickness between them. A possible reason for this difference may be the higher carbon content in PS steel than QST steel. In a study on the propagation of corrosion in embedded reinforcements, Li, et al.,[1] observed that the corrosion rate of conventional steel bars (analogous to the QST steel evaluated in this study) was higher than that of unstressed prestressing strands at similar conditions. They suggested that it could be because of the higher carbon content in the latter which can provide more corrosion cathodes so that "more passivating reactions occur" based on Zhu.[80] The differences may also be attributed to the presence of higher amount of alloying elements such as chromium, which acts in favor of passivation (refer Table 1). Further, during the P-to-A transition, the reduction in R_{ox} of QST system was found to be gradual (950 kΩ·cm^2 → 353 kΩ·cm^2) in contrast with that of PS system (1,573 kΩ·cm^2 → 537 kΩ·cm^2), as discussed earlier based on the qualitative analysis. This trend matched exactly with the Q_{ox} parameter increasing gradually in QST system over the duration of exposure. In case of PS system, Q_{ox} was found to increase suddenly between 56 d and 70 d. The P-to-A transition in QST and PS steels occurred at the end of 10.4±1.7 and 9.2±1.5 cycles, respectively. The number of cycles upto P-to-A transition, of QST steel in OPC mortar subjected to cyclic wet-dry exposure to SPS+3.5% NaCl, is consistent with previous reports (i.e., ≈ 7 to 9).[55] The number of cycles until P-to-A transition can thus be considered as statistically similar for the QST and PS steels although the protection offered by the passive film in PS steel was better initially. However, the resulting

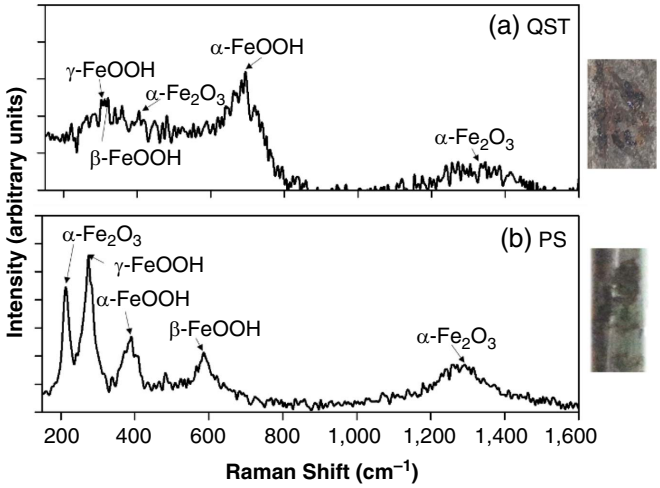

Lepidocrocite (γ-FeOOH)- 250, 300, 379, 476, 685
Goethite (α-FeOOH)- 244, 299, 385, 480, 548, 681
Akaganeite (β-FeOOH)- 310, 390, 500, 534, 615, 720
Hematite (α-Fe_2O_3)- 225, 289, 404, 1,310
Maghemite (γ-Fe_2O_3)- 665, 720, 1,598
Magnetite (Fe_3O_4)- 532, 670

FIGURE 8. *Raman spectrography results of corrosion products collected from QST and PS steels embedded in OPC mortar after detection of P-to-A transition.*

increase in corrosion was more significant for the PS steel at the transition from passive to active behavior.

To identify the cause of this contradictory behavior, the surface residual stresses on the QST and PS steels were measured. A compressive residual stress was observed on the surface of QST steel with the magnitude being 89±5 MPa and 11±4 MPa (on and between ribs, respectively). This can be attributed to the quenching process involved in the manufacturing of QST steel. When the steel bar is quenched, the surface undergoes martensitic transformation. A compressive residual stress may develop on the surface if the net plastic strain generated in the region of thermal contraction (core) is greater than that generated in the transformational region (surface).[81] The QST has a compressive surface residual stress, and in stainless steels, a compressive surface residual stress is reported to improve passivity, suggesting that the passive film formed on carbon steel in alkaline environments may be similarly enhanced by a compressive surface residual stress.[82] A lower passive corrosion current density, and higher breakdown potentials are also reported in aluminum alloys with compressive residual stress.[83]

On the contrary, residual tensile stresses of 68±14 MPa and 49±6 MPa were observed on the PS steel along the longitudinal and radial directions, respectively. This can be attributed to the process of cold drawing by which PS steel is manufactured.[7] Although low-relaxation strands, such as the one used in this study, are subjected to heat treatment after the drawing, a residual surface tensile stress was still observed. As reported by Lu, et al., even a tensile stress "well below" the yield strength can result in a passive film with defects and low resistance to breakdown.[84]

Nanoscale characterization of passive films of iron in alkaline environments reveal a multilayer film structure with inner oxide layers (Fe^{2+}-rich) and outer oxide layers (Fe^{3+}-rich).[46,85-86] According to DorMohammadi, et al.,[86] theoretical passivity models suggest that the inner layer is formed on the metal substrate while the outer layer forms through hydrolysis of cations that are ejected from the inner layers. The tensile residual stresses measured at the surface of unstressed PS was within 70 MPa, which is just about 4% of the ultimate tensile strength of 1,800 MPa. While it is well agreed upon that a tensile stress causes a weak oxide coverage, the authors believe that the effect of this low-magnitude residual tensile stress could be more predominant on the inner oxide layer and reduce as the subsequent layers are formed. Hence, the authors believe that the influence of surface stress state is predominant only in the inner oxide layers at proximity to the steel surface. This theory explains why the bulk response of passive film is better for PS steel than QST steel despite the influence of the stress state (unfavorable and favorable in the respective steels). In such a case, the steel/passive film interface of PS steel is significantly weaker than the bulk passive film while the opposite holds true for QST steel. Because of this, the passive film of QST steel remains integrated after depassivation with the dissolution of the exposed metal only. On the other hand, the passive film on PS steel may crack due to the flow of corrosion products through the defects in the inner passive film. This also explains why the cracks were along both the longitudinal and radial directions. Further studies on the passive film growth in both PS and QST steels and interaction with chloride ions can throw more light into the mechanism. Mott-Schottky analysis would be very useful for getting further insights into the mechanism of P-to-A transition in steel-cementitious (sol-gel) system. However, authors believe that the selection of test parameters for Mott-Schottky analysis for steel-cementitious system may not be as straightforward/conventional as in steel-solution systems and, hence, have kept this out-of-scope in this paper.

Further, an EDAX analysis performed on the surface of an as-received PS steel king wire degreased with ethanol is shown in Figure 9. It can be observed that the intensity of zinc, phosphorous, and oxygen peaks varied in the troughs and crests formed during the contact of the cold drawing dies with the steel. The corrosion resistance of phosphate coatings is generally a few times higher than that of the substrate.[87] These heterogeneities on the surface of the PS steel may contribute to a nonuniform passive film formation over the surface of PS

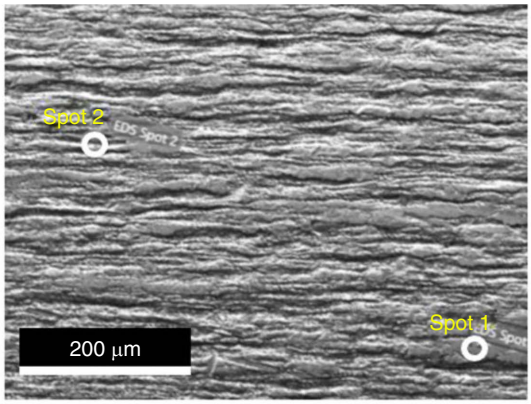

Element wt%	Fe	O	P	Zn
Spot 1	94.47	1.06	0.10	-
Spot 2	56.09	10.42	5.35	13.59

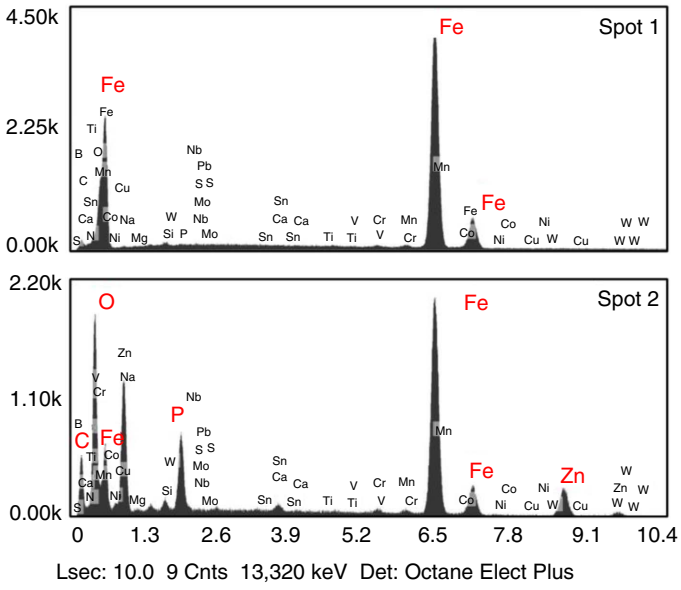

FIGURE 9. *EDAX analysis of the surface of PS king wire in "as-received" condition.*

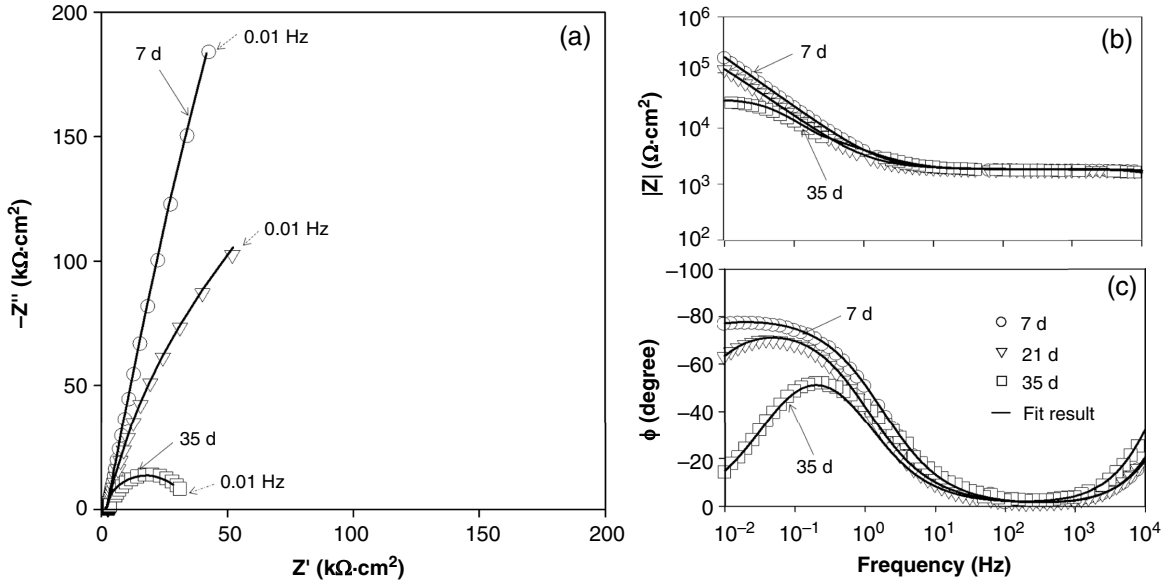

FIGURE 10. *Typical evolution of the impedance response at E_{corr} (AC amplitude: ±10 mV [peak-to-peak]) obtained at the end of wet exposure to SPS+2% NaCl for stressed PS steel in OPC mortar. (a) Nyquist, (b) Bode magnitude, and (c) Bode phase representations.*

steel. It is well known that corrosion initiation in PS wires can occur at the imperfections on the zinc phosphate-coated surface, which can arise from the cold-drawing or stranding operations.[43] The line and surface roughness of the PS steel king wire used in this study are reported to be 712 µm and 25 µm, respectively.[88] A reduction in the roughness could be favorable for formation of a more uniform passive film.[44]

From Phase 1, it could be concluded that the chemical composition, stress state, and surface microstructure can play synergistic roles in the P-to-A transition of steel reinforcements in cementitious systems. In addition, the depassivation of PS steel in simulated alkaline solutions is reported to depend on stress level, chloride concentration, temperature, and oxygen availability at the steel surface.[41] The effect of stress on the P-to-A transition of PS in OPC-based mortar was evaluated in Phase 2 of the study.

3.2 | Phase 2: Effect of Stress on the P-to-A Transition of Prestressing Steels

3.2.1 | Electrochemical Impedance Spectroscopy and E_{corr} Responses

A typical evolution of the impedance response for stressed PS steel embedded in OPC mortar and subjected to cyclic wet and dry exposure in SPS+2% NaCl is shown in Figure 10. The P-to-A transition was found to be like that of the unstressed case, with the drastic reduction in both the slope of the Nyquist response (from 10^0 to 10^{-2} Hz) and $|Z|_{0.01\ Hz}$ observed with increasing duration of exposure. Micrograph and line sketch shown in Figures 11(a) and (b) indicate passive film cracking with similar flaky corrosion products appearing to be disintegrating the passive film. The composition of the passive film at the cracked location on PS_0.76 f_{pu} after P-to-A transition, as determined using EDAX, is shown in Figure 12. F, O, and Cl were found to be present at large amounts. This strengthens the theory that it is the passive film that is cracked in the presence of chlorides. Also, another location within the cracked region where the flaky corrosion products are visible is highlighted.

The evolution of E_{corr} with the duration of exposure to chlorides for each test specimen is shown in Figures 13(a) and (c). In every case, the E_{corr} drastically transitioned from "noble" values of say more than −200 mV_{SCE} to "active" values of less than −400 mV_{SCE}. The variation in the normalized $|Z|_{0.01\ Hz}$ (calculated as the ratio of $|Z|_{0.01\ Hz}$ measured at the current cycle over that measured at the first cycle) was found to follow a similar trend for all of the specimens, as shown in Figures 13(b) and (d). The data on low-frequency impedance modulus of each specimen was normalized with respect to its low-frequency impedance modulus obtained at the first cycle of exposure. This helped in bringing all of the data to within a range of 0 to 1 and visualizing the percent change in surface degradation during the P-to-A transition of all of the specimens. Normalization also helped in viewing the data from all of the specimens in one window and understanding that all specimens do provide similar trend indicating reasonable repeatability of the measurements. In addition, the trend of evolution of the E_{corr} over the test duration was found to be consistently similar to that of the variation in the spectra. The drop in both E_{corr} and normalized $|Z|_{0.01\ Hz}$ occurred at the same cycle of exposure, indicating an unambiguous correlation between the E_{corr} measurements and the change in the passive film integrity (integrated to cracked). That is, the initial measurements correspond to a well passivated system (similar to the one shown in Figure 7[b]) and the last two measurements correspond to PS with cracked passive film (as shown in Figures 7[c] through [f]). Fit results shown in Table 4 reveal that the R_{ox} of stressed PS steel system was higher initially (3,604 kΩ·cm²) compared to that of the unstressed PS system (1,573 kΩ·cm²). The initial Q_{ox} values for the stressed system (62 mS·s^{n2}/cm²) was also lower than that of the unstressed system (122 mS·s^{n2}/cm²). The reason for this unexpected behavior may be attributed to the plastic deformations within the microstructure of the pearlitic steel due to the application of prestress, which may positively influence the initial passivation reactions. Further, microstructural investigations can throw more light into the mechanism. Further, similar to the case of unstressed PS steel, the stressed PS steel system exhibited sudden increase and decrease in the Q_{ox}

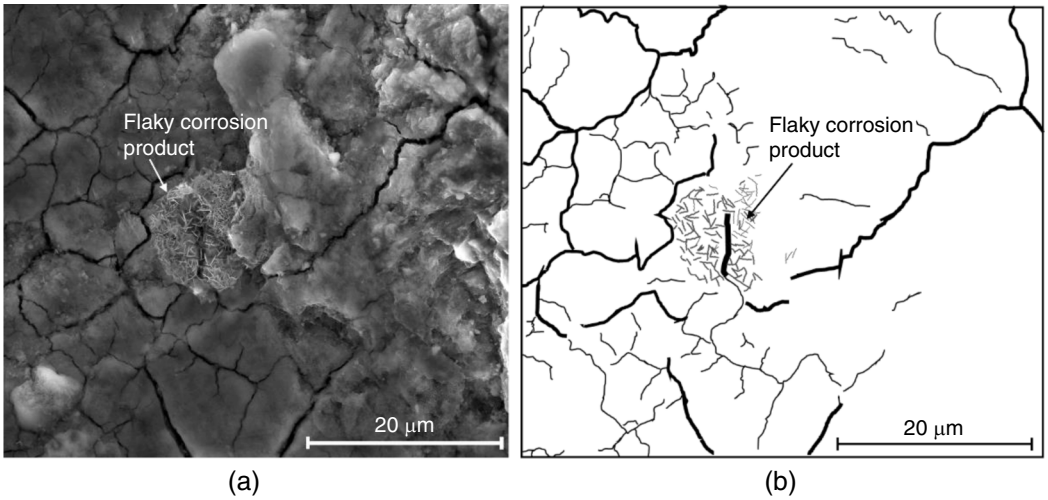

FIGURE 11. *Passive film cracking observed on stressed PS steel in OPC-based mortar after 35 d of cyclic exposure to SPS+2% NaCl. (a) Micrograph and (b) line sketch.*

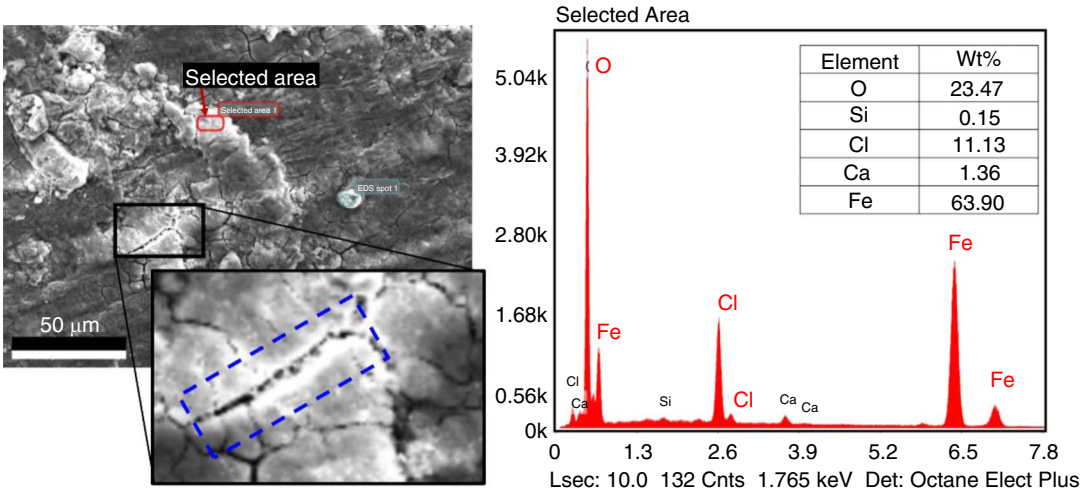

FIGURE 12. *EDAX analysis of the cracked passive film.*

and R_{ox} values, respectively, during the P-to-A transition. However, although the pattern of P-to-A transition was found to be similar for both the unstressed and stressed systems considered, the duration of exposure to chlorides until cracking was different. As stated before, the exposure solution was kept less aggressive for the stressed systems (SPS+2% NaCl) than the unstressed systems (SPS+3.5% NaCl) because of a previous experience with very early initiation in the former when exposed to SPS+3.5% NaCl. Despite this, the passive film on the stressed steel was found to crack at less number of cycles than the unstressed steel, indicating a reduction in chloride concentration required for P-to-A transition in the presence of stress.

3.2.2 | Chloride Threshold

Figure 14 shows the Chloride Threshold (Cl_{th}) of unstressed and stressed PS steels. The determined values are within the range reported for unstressed PS steel in cementitious media, which is 0.006% to 1.4% by weight of binder (%bwob).[89] In the presence of design prestress of 0.76 f_{pu}, the Cl_{th} reduced by about 50%. This may be due to the formation of a defective passive film in the presence of tensile stress,[84] as explained earlier. However, the defect density in the inner passive film is expected be higher in the stressed case than the unstressed case due to the higher magnitude of tensile stress in the former, at the time of passivation. It is to be noted that the scatter in the Cl_{th} data is higher for the stressed systems than unstressed. Also, considering that P-to-A transition is the first step toward the crack initiation phase of SCC with subsequent propagation and failure, as discussed earlier, the amount of chlorides that can be considered as "aggressive enough to cause initiation of SCC" can be said to be lower in the presence of stress. Therefore, this aspect should be considered in the durability-based design of PTC structures to avoid initiation of SCC. The Cl_{th} can also be dependent on the passivating environments provided by various cementitious systems such as pulverized fuel ash, ground granulated blast furnace slag, limestone calcined clay cement, etc. due to the differences in chemistry,[46] pH,[42] and alterations in the pore structure of the interface.[90] Also, if the absorption of H_{ad} is favored in the cracked locations, passive film cracking in PS

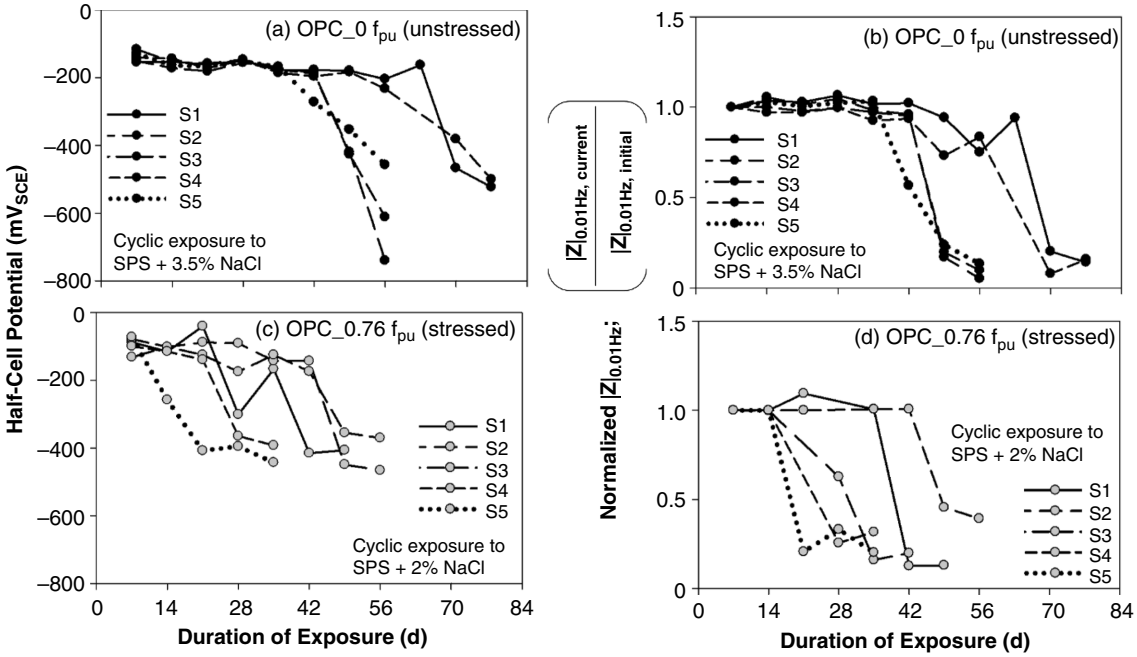

FIGURE 13. *Variation in E_{corr} and normalized $|Z|_{0.01\ Hz}$ of PS in OPC. (a) and (b) OPC_0 f_{pu} (unstressed) and (c) and (d) OPC_0.76 f_{pu} (stressed).*

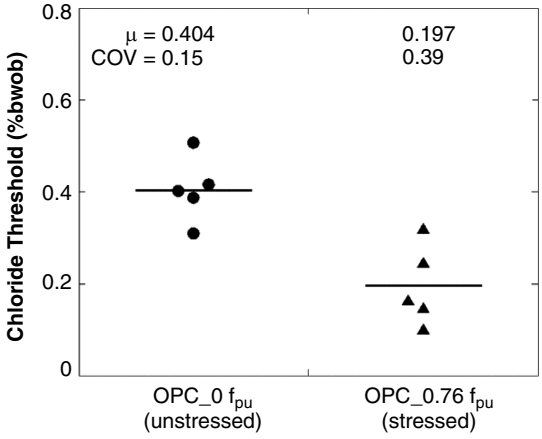

FIGURE 14. *Chloride threshold of PS steel in OPC.*

can be a potential precursor to hydrogen-induced SCC in PTC systems. This aspect needs to be studied in detail and is out of the scope of this paper.

CONCLUSIONS

In this study, EIS tests were conducted on various steel-cementitious specimens. EIS spectra from the conventional QST steel and the unstressed and stressed prestressing (PS) steels embedded in OPC-based cement mortar and gradually exposed to chloride solutions were obtained. The changes in the EIS spectra as a function of exposure time were monitored and passive-to-active (P-to-A) transition mechanisms were investigated. The following are the major conclusions drawn.

➢ The P-to-A transition of PS and QST steels can be characterized using the low-frequency impedance modulus, i.e., $|Z|_{0.01\ Hz}$ and the slope of the EIS response in low-frequency region (10^{-1} Hz to 10^{-2} Hz). Based on these parameters, the quality of passive film on PS steel is found to be better than that on QST steel in the absence of chlorides. This can be attributed to the metallurgical factors such as the stress state, chemical composition, and surface microstructure.

➢ The P-to-A transition of QST and PS steels are gradual and drastic, respectively, when embedded in cement mortar and exposed to chlorides. This is because the P-to-A transition in QST and PS steels are governed by conventional pitting and passive film cracking mechanisms, respectively. The possible reasons for the differences are postulated to be the presence of defects in the inner layer of passive film formed on the PS steel with cold-drawing induced tensile residual stresses and the possibility of higher crystalline fraction in the corrosion products formed on the PS steel compared to QST.

➢ The presence of prestress does not change the pattern of P-to-A transition, but can reduce the chloride threshold by 50%, when embedded in OPC concrete. The amount of chlorides that can cause the initiation of SCC of PS steels in cementitious systems can be considered as the chloride threshold (Cl_{th}) of PTC systems. For prestressed steels in OPC system, this is about 0.2% Cl^- by weight of binder. The choice of the steel and binder and the stress level can influence this parameter.

ACKNOWLEDGMENTS

The authors acknowledge the financial support from the Department of Science and Technology (DST), Government of India (SERB Sanction No. EMR/2017/004687). The financial support from the Ministry of Human Resources Development, Government of India, and the Department of Civil Engineering, Indian Institute of Technology Madras (IIT Madras), Chennai is also acknowledged. The support from laboratory staff in the Construction Materials Research Laboratory, the Civil Engineering Department Workshop, SEM and XRD facilities in Department of Metallurgical and Materials Engineering, and Confocal Raman Spectroscopy facility in the Department of Physics, at IIT Madras, is highly appreciated.

References

1. F. Li, Y. Yuan, C.Q. Li, *Constr. Build. Mater.* 25 (2011): p. 3878-3885.
2. R.A. Rogers, M. Al-Ani, J.M. Ingham, "Assessing Pre-Tensioned Reinforcement Corrosion Within the New Zealand Concrete Bridge Stock," NZ Transport Agency research report 502, 2013.
3. C. Sly, *J. Fail. Anal. Prev.* 1 (2001): p. 7-9.
4. S.M. Bruce, P.S. McCarten, S.A. Freitag, L.M. Hasson, "Deterioration of Prestressed Concrete Bridge Beams," Austroads Bridge Conference (Perth, Australia: Austroads, 2006).
5. CUR, "Cases of Damage Due to Corrosion of Prestressing Steel," CUR report no. 49, 1971.
6. V. Novokshchenov, *Corrosion* 50 (1994): p. 477-485.
7. ACI 222.2R-01, "Corrosion of Prestressing Steels (Reapproved 2010) (concrete.org)," Technical document (Farmington Hills, MI: American Concrete Institute, 2001).
8. Fib bulletin 26, "Influence of Material and Processing on Stress Corrosion Cracking of Prestressing Steel," Technical report, Fédération internationale du béton, Lausanne, Switzerland, 2003, https://doi.org/10.35789/fib.BULL.0026.
9. L. Vehovar, V. Kuhar, A. Vehovar, *Eng. Fail. Anal.* 5 (1998): p. 21-27.
10. J. Toribio, E. Ovejero, *Mech. Time-Dependent Mater.* 1 (1998): p. 307-319.
11. D.G. Enos, J.R. Scully, *Metall. Mater. Trans. A Phys. Metall. Mater. Sci.* 33 (2002): p. 1151-1166.
12. Y. Zhao, Y. Tan, X. Ji, Z. Xiang, Y. He, S. Xiang, *Mater. Sci. Eng. A* 731 (2018): p. 93-101.
13. D.G. Enos, A.J. Williams, J.R. Scully, *Corrosion* 53 (1997): p. 891-908.
14. W.H. Hartt, C.C. Kumria, R.J. Kessler, *Corrosion* 49 (1993): p. 377-385.
15. M.J. Szeliga, ed., *Corrosion in Prestressed Concrete: Pipes, Piles and Decks* (Houston, TX: NACE International, 1995).
16. N.A. Vu, A. Castel, R. François, *Corros. Sci.* 51 (2009): p. 1453-1459.
17. R.H. Jones, *Stress Corrosion Cracking: Materials Performance and Evaluation* (Materials Park, OH: ASM International, 1992).
18. J. Sanchez, J. Fullea, C. Andrade, C. Alonso, *Corros. Sci.* 49 (2007): p. 4069-4080.
19. R.M. Schroeder, I.L. Müller, *Corros. Sci.* 45 (2003): p. 1969-1983.
20. K. McGuinn, J.R. Griffiths, *Br. Corros. J.* 12 (1977): p. 152-157.
21. K.F. McGuinn, M. Elices, *Br. Corros. J.* 16 (1981): p. 187-195.
22. S. Ramadan, L. Gaillet, C. Tessier, H. Idrissi, *Appl. Surf. Sci.* 254 (2008): p. 2255-2261.
23. M.C. Alonso, R.P.M. Procter, C. Andrade, M. Sáenz de Santa María, *Corros. Sci.* 34 (1993): p. 961-973.
24. M. Perrin, L. Gaillet, C. Tessier, H. Idrissi, *Corros. Sci.* 52 (2010): p. 1915-1926.
25. M. De Abreu, M. Iordachescu, A. Valiente, *Constr. Build. Mater.* 66 (2014): p. 38-44.
26. M. Ichiba, J. Sakai, T. Doshida, K. Takai, *Scr. Mater.* 102 (2015): p. 59-62.
27. J. Toribio, *Mater. Des.* 18 (1997): p. 81-85.
28. J. Mietz, B. Isecke, *Mater. Corros.* 53 (2002): p. 373-384.
29. R.N. Parkins, M. Elices, V. Sanchez-Galvez, L. Caballero, *Corros. Sci.* 22 (1982): p. 379-405.
30. M. Elices, L. Caballero, A. Valiente, J. Ruiz, A. Martin, *Corrosion* 64 (2008): p. 164-174.
31. B. Isecke, J. Miletz, *Steel Res.* 64 (1993): p. 97-101.
32. W. Vélez, F. Matta, P. Ziehl, *Mater. Struct.* 49 (2016): p. 507-520.
33. J. Karuppanasamy, R.G. Pillai, *Corrosion* 73 (2017): p. 1119-1131.
34. ASTM G5, "Standard Reference Test Method for Making Potentiodynamic Anodic Polarization" (West Conshohocken, PA: ASTM International, 2015).
35. J. Williamson, O.B. Isgor, *Adv. Civ. Eng. Mater.* 5 (2016): p. 20150031.
36. Y.M. Chen, M.E. Orazem, *Corros. Sci.* 104 (2015): p. 26-35.
37. X. Feng, Y. Tang, Y. Zuo, *Corros. Sci.* 53 (2011): p. 1304-1311.
38. J. Sánchez, J. Fullea, C. Andrade, J.J. Gaitero, A. Porro, *Corros. Sci.* 50 (2008): p. 1820-1824.
39. M.F. Montemor, A.M.P. Simões, M.M. Salta, *Cem. Concr. Compos.* 22 (2000): p. 175-185.
40. NACE TM0169/G31, "Standard Guide for Laboratory Immersion Corrosion Testing of Metals" (Houston, TX: NACE, 2012).
41. B. Díaz, L. Freire, X.R. Nóvoa, M.C. Pérez, *Electrochim. Acta* 54 (2009): p. 5190-5198.
42. R.D. Moser, P.M. Singh, L.F. Kahn, K.E. Kurtis, *Corros. Sci.* 57 (2012): p. 241-253.
43. R.D. Moser, P.M. Singh, L.F. Kahn, K.E. Kurtis, *Corrosion* 67 (2011): p. 1-14.
44. G.S. Duffó, S.B. Farina, *Cem. Concr. Res.* 88 (2016): p. 211-216.
45. A. Poursaee, C.M. Hansson, *Cem. Concr. Res.* 37 (2007): p. 1127-1133.
46. H.B. Gunay, P. Ghods, O. Isgor, J.C.C. Carpenter, X. Wu, *Appl. Surf. Sci.* 274 (2013): p. 195-202.
47. U. Angst, B. Elsener, C.K. Larsen, Ø. Vennesland, *Cem. Concr. Res.* 39 (2009): p. 1122-1138.
48. J. Wu, H. Li, Z. Wang, J. Liu, *Constr. Build. Mater.* 112 (2016): p. 733-738.
49. M. Otieno, G. Golden, M.G. Alexander, H. Beushausen, *Mater. Struct. Constr.* 52 (2019): p. 1-14.
50. S. Rengaraju, R.G. Pillai, R. Gettu, L. Neelakantan, *Corrosion* 77 (2021): p. 445-459.
51. R.G. Pillai, P. Gardoni, D. Trejo, M.B.D. Hueste, K.F. Reinschmidt, *J. Mater. Civ. Eng.* 22 (2010): p. 967-977.
52. I. Fayala, L. Dhouibi, X.R. Nóvoa, M. Ben Ouezdou, *Cem. Concr. Compos.* 35 (2013): p. 181-189.
53. G.R. Meira, C. Andrade, E.O. Vilar, K.D. Nery, *Constr. Build. Mater.* 55 (2014): p. 289-298.
54. H. Wu, *Adv. Cem. Res.* 26 (2014): p. 292-301.
55. S. Rengaraju, L. Neelakantan, R.G. Pillai, *Electrochim. Acta* 308 (2019): p. 131-141.
56. D.V. Ribeiro, J.C.C. Abrantes, *Constr. Build. Mater.* 111 (2016): p. 98-104.
57. D. Koleva, K. van Breugel, J.H. de Wit, A.L. Fraaij, N. Boshkov, *ECS Trans.* 2 (2007): p. 51-62.
58. K. Darowicki, J. Orlikowski, A. Arutunow, *Electrochim. Acta* 48 (2003): p. 4189-4196.
59. D.M. Bastidas, *Corrosion* 63 (2007): p. 515-521.
60. K. Darowicki, S. Krakowiak, P. Ślepski, *Electrochim. Acta* 49 (2004): p. 2909-2918.
61. J. Flis, H.W. Pickering, K. Osseo-Asare, *Electrochim. Acta* 43 (1998): p. 1921-1929.
62. X. Feng, Y. Zuo, Y. Tang, X. Zhao, J. Zhao, *Corros. Sci.* 65 (2012): p. 542-548.
63. U. Martin, J. Ress, J. Bosch, D.M. Bastidas, *Electrochim. Acta* 335 (2020): p. 1-13.
64. IS 14268, "Uncoated Stress Relieved Low Relaxation Seven-Wire (Ply) Strand for Prestressed Concrete—Specification (First Revision)," Bureau of Indian Standards, New Delhi, India, 2017.
65. L. Calabrese, G. Campanella, E. Proverbio, *Corros. Sci.* 73 (2013): p. 161-171.
66. IS 1786, "High Strength Deformed Steel Bars and Wires for Concrete Reinforcement - Specification" (New Delhi, India: Bureau of Indian Standards, 2008).
67. IS 12269, "Ordinary Portland Cement, 53 Grade - Specification" (New Delhi, India: Bureau of Indian Standards, 2013).
68. IS 650, "Specification for Standard Sand for Testing of Cement" (New Delhi, India: Bureau of Indian Standards, 1991).
69. IS 1343, "Prestressed Concrete-Code of Practice" (New Delhi, India: Bureau of Indian Standards, 2012).
70. S. Rengaraju, "Electrochemical Response and Chloride Threshold of Steel in Highly Resistive Concrete Systems" (Ph.D. thesis diss., submitted to Indian Institute of Technology Madras, 2019).
71. SHRP S332, "Standard Test Method for Chloride Content in Concrete Using the Specific Ion Probe," in *Condition Evaluation of Concrete Bridges Relative to Reinforcement Corrosion-Volume 8: Procedure Manual*, SHRP-S/FR-92-110 (Washington, DC: Strategic Highway Research Program, 1992), p. 85–102.
72. D. Trejo, D. Miller, "System and Method for Determining the Chloride Corrosion Threshold Level for Uncoated Steel

Reinforcement Embedded in Cementitious Material," U.S. patent application no. 60/288, 210, 2002.
73. D. Trejo, R.G. Pillai, *ACI Mater. J.* 100 (2003): p. 519-527.
74. J. Karuppanasamy, R.G. Pillai, *Mater. Struct. Constr.* 50 (2017): p. 1-17.
75. O. Poupard, A. Aït-Mokhtar, P. Dumargue, *Cem. Concr. Res.* 34 (2004): p. 991-1000.
76. R.G. Kelly, J.R. Scully, D. Shoesmith, R.G. Buchheit, *Electrochemical Techniques in Corrosion Science and Engineering* (Boca Raton, FL: CRC Press, 2002).
77. D.M. Bastidas, J. Ress, U. Martin, J. Bosch, A. La Iglesia, J.M. Bastidas, *Rev. Met.* 56 (2020): p. 1-15.
78. D. Tuschel, "Why Are the Raman Spectra of Crystalline and Amorphous Solids Different?," *Spectroscopy*, January 3, 2017 (2017), https://www.spectroscopyonline.com/view/why-are-raman-spectra-crystalline-and-amorphous-solids-different.
79. A. Sánchez-Deza, D.M. Bastidas, A. La Iglesia, E.M. Mora, J.M. Bastidas, *Rev. Met.* 54 (2018): p. 1-10.
80. R.Z. Zhu, *Corrosion Science of Metals* (Berlin, Germany: Springer, 1989) [in Chinese].
81. M.T. Todinov, *Model. Simul. Mater. Sci. Eng.* 6 (1998): p. 273-291.
82. O. Takakuwa, H. Soyama, *Adv. Chem. Eng. Sci.* 5 (2015): p. 62-71.
83. X. Liu, G.S. Frankel, *Corros. Sci.* 48 (2006): p. 3309-3329.
84. B.T. Lu, Y. Zeng, X. Pang, J.L. Luo, *Corros. Eng. Sci. Technol.* 50 (2015): p. 186-190.
85. P. Ghods, O.B. Isgor, G.J.C. Carpenter, J. Li, G.A. McRae, G.P. Gu, *Cem. Concr. Res.* 47 (2013): p. 55-68.
86. H. DorMohammadi, Q. Pang, P. Murkute, L. Árnadóttir, O.B. Isgor, *Npj Mater. Degrad.* 3 (2019): article 19.
87. A. Stankiewicz, "Self-Healing Nanocoatings for Protection against Steel Corrosion," in *Nanotechnology in Eco-Efficient Construction*, 2nd ed., Materials, Processes and Applications, Woodhead Publishing Series in Civil and Structural Engineering (Amsterdam, The Netherlands: Elsevier, 2019), p. 303-335.
88. A. Biswal, "Parameters Affecting the Service Life of Prestressed Concrete Systems" (Masters' thesis diss., submitted to Indian Institute of Technology Madras, 2020).
89. P.Y. Virmani, H. Ghasemi, "Literature Review of Chloride Threshold Values for Grouted Post-Tensioned Tendons," FHWA Publ. No. FHWA-HRT-12-067, 2012, http://www.fhwa.dot.gov/research/.
90. D. Joseline, R.G. Pillai, *Indian Concr. J.* 94 (2020): p. 54-67.

NOMENCLATURE

PTC	Pretensioned concrete
PS	Prestressing
QST	Quenched and self-tempered
SCC	Stress corrosion cracking
P-to-A	Passive-to-Active
Cl_{th}	Chloride threshold
f_{pu}	Ultimate tensile strength
OPC	Ordinary Portland cement
SPS	Simulated pore solution
EIS	Electrochemical impedance spectroscopy
SEM	Scanning electron microscopy
EDAX	Energy dispersive x-ray analysis
XRD	X-ray diffraction
E_{corr}	Open-circuit potential
$\|Z\|_{0.01\ Hz}$	Impedance modulus corresponding to 0.01 Hz
$\varphi_{0.01\ Hz}$	Phase angle corresponding to 0.01 Hz
%bwob	% by weight of binder